AIAA SciTech 2018
8 - 12 Jan 2018, Kissimmee, FL
AIAA-2018-2047

Investigation of Flow Dynamics Over Turrets with Different Spanwise Aspect Ratios Using PSP

Nicholas De Lucca[1], Stanislav Gordeyev[2], Jacob Morrida[3] and Eric J. Jumper[4]
University of Notre Dame, Notre Dame, IN, 46556

Unsteady pressure fields on and around turrets with the same streamwise curvature, but different spanwise extents were measured using a fast-response pressure sensitive paint and multiple high-speed cameras. Data were collected over a range of incoming Mach numbers between 0.4 and 0.68. POD and DMD techniques were used to analyze the dynamics and the topology of the wakes for different turret geometries and incoming speeds. The spectrum of the first POD mode, which is associated with the wake shifting mode, was found to scale with the spanwise extent of the turret. The spectra of the second and the third POD mode, associated with the wake breathing mode, scaled with the streamwise radius of curvature. The presence of an unsteady shock on top of both turret geometries at high transonic speeds was found to have an organizing effect on the separated flow, evidenced by the increased correlations between the convecting structures in the wake and the shock-induced separation and appearance of spectral peaks for dominant POD modes.

I. Introduction

Directed energy and free-space communications systems that can be operated on aircraft are desirable and hemispherical turret systems are geometries of choice for maximizing field-of-regard. In the last decade, there has been substantial work done on these hemispherical turret systems to determine the aerodynamic [1,2,3] and aero-optic performance [4,5,6]. CFD has also been extensively used to predict the dynamic and aero-optical performance of turrets [7,8,9,10,11]. While it was a significant progress quantifying aero-optical distortions caused by the turret wake [4,5,6], details of the dynamics of the wake itself are still not quite clear at this moment. Furthermore, at high transonic speeds, an unsteady shock appears on top of the turret [12] and the shock forces the flow to separate prematurely [13]; the shock-induced effect on the dynamics of the wake are also under investigation.

Both the hemisphere and a wall-mounted spanwise cylindrical turret have surface curvature in the streamwise direction, which is the main mechanism for the flow to separate downstream of both geometries. As a consequence, there has been substantial work on spanwise-cylindrical [14,15,16] turrets as a simplified but still relevant geometry to understand the wake dynamics, at subsonic and transonic speeds. While aero-optical effects of the separated wake were found to be similar for both geometries, the wake dynamics are not the same due to the presence of spanwise surface curvature for hemispheres. For instance, at transonic speeds, hemispherical turrets were

[1] Post-Doctoral Researcher, Department of Aerospace and Mech. Eng., Student AIAA Member
[2] Associate Professor, Department of Aerospace and Mech. Eng., AIAA Associate Fellow
[3] Graduate Research Assistant, Department of Aerospace and Mech. Eng., Student AIAA Member
[4] Professor, Department of Aerospace and Mech. Eng., AIAA Fellow

shown to have a shock formed at a viewing angle of 84°-87°, while the shock on cylindrical turrets was observed further downstream at 95°-100° [14].

One consequence of the spanwise curvature is that the incoming boundary layer primarily goes around the hemisphere on both sides and forms a necklace vortex downstream of the hemisphere [12]. Another feature of the wake topology downstream of the hemisphere are two "horn" vortices, formed on the back of the hemisphere [12]. Both the necklace and the "horn" vortices are the consequence of the spanwise curvature and therefore not present downstream of the wall-mounted spanwise cylindrical turrets. These vortices create a strong downwash effect via Biot-Savart induction, forming a "quiet valley" on the back portion of the hemisphere [6], among other effects. One way to study the effect of these vortices on the wake dynamics is to start separating these vortices in the spanwise direction, thereby weakening the downwash effect. It can be accomplished by studying the wake dynamics for intermediate geometries, when the hemisphere is "morphed" into the spanwise cylindrical turret by adding progressively wider cylindrical segments to the middle of the hemisphere to change its spanwise extent, while keeping the same streamwise curvature. In this case, the effect of the streamwise curvature, which causes the flow to separate, and the effect of the necklace and the "horn" vortices, which create significant 3-dimensional effects in the wake, can be separated and properly studied.

Recent advances in fast-response Pressure Sensitive Paint (PSP) allows studying a full spatio-temporal pressure field on and around the turret. PSP measurements are based on oxygen-sensing molecules known as luminophore, which fluoresce when exposed to ultraviolet light [17,18]. Oxygen quenches the luminescence of the paint, so as the air pressure increases, the oxygen concentration increases, which reduces the light emission. Therefore, the paint gets brighter as pressure decreases.

The pressure field around turrets has been studied in the past using PSP [3,19,20]. In these PSP studies, the pressure field only on the turret itself was measured and studied. Recent studies [21,22] included the pressure measurements on and around the turret to better understand the wake dynamics downstream of the turrets at different subsonic and transonic speeds, the latter ones allow studying the effect of the unsteady shock forming on top of the turret.

In this paper, fast-response PSP was used to study the similarities and differences in the unsteady pressure fields between the turrets with different spanwise extent at various subsonic and transonic speeds. Using measured global pressure fields, different dominant pressure modes on and around turrets with different spanwise extents were extracted and analyzed using Proper Orthogonal Decomposition (POD) and Dynamic Mode Decomposition (DMD) techniques. This work expands upon recent research that has investigated the relationship between the shock location over the turret and the wake of the turret [21,22,23,24].

II. Experimental Setup

The PSP experiment was performed in the Whitefield Wind Tunnel facility at the University of Notre Dame. This facility contains a 3'x3' wind tunnel that is capable of up to M = 0.7 flow. Two models were, a 8"-diameter hemisphere, shown in Figure 1, left, and another turret model, consisted of a hemispherical base of the same 8"-diameter with cylindrical segments added in to increase the spanwise aspect ratio of the turret, see Figure 1, right. The aspect ratio, AR, is defined is a ratio between the spanwise and streamwise lengths of the turret. Thus, the hemisphere-only turret corresponded to AR = 1, and the second turret had a larger AR = 1.9. Later in the paper the second geometry will be referred as the AR = 1.9 turret. Table 1 contains the geometric values and run conditions for each turret configuration. Due to different blockage values and turbulent wakes,

the maximum Mach number for each configuration was dependent on the configuration itself; the larger aspect ratio had the larger blockage and thus the lower achievable Mach number. Unsteady pressure fields were studied at different incoming speeds; these speeds were compensated for the blockage effects and reported in Table 1 for different turret geometries.

A schematic and picture of the PSP setup are shown in Figure 2. A fast response Polymer-ceramic/PtTFPPF PSP formulation from ISSI (Product ID: FP-XXX) was used to measure the surface pressure field on the turrets and in the wake behind the turrets. The PSP was illuminated using eight UV light sources that emit in a narrow band about 400 nm. The UV lights were aligned with quartz inserts in the tunnel, Figure 5 bottom, to minimize absorption and reflection of the UV light. The PSP images were taken using three Phantom brand high-speed cameras. The three cameras used, shown in Figure 5, left, were a v1611 (Camera 1), a v1610 (Camera 2) and a v711 (Camera 3). Additionally, several 10 PSI differential Kulite sensors were placed both along the centerline on the turrets and in the wake to perform in-situ calibration.

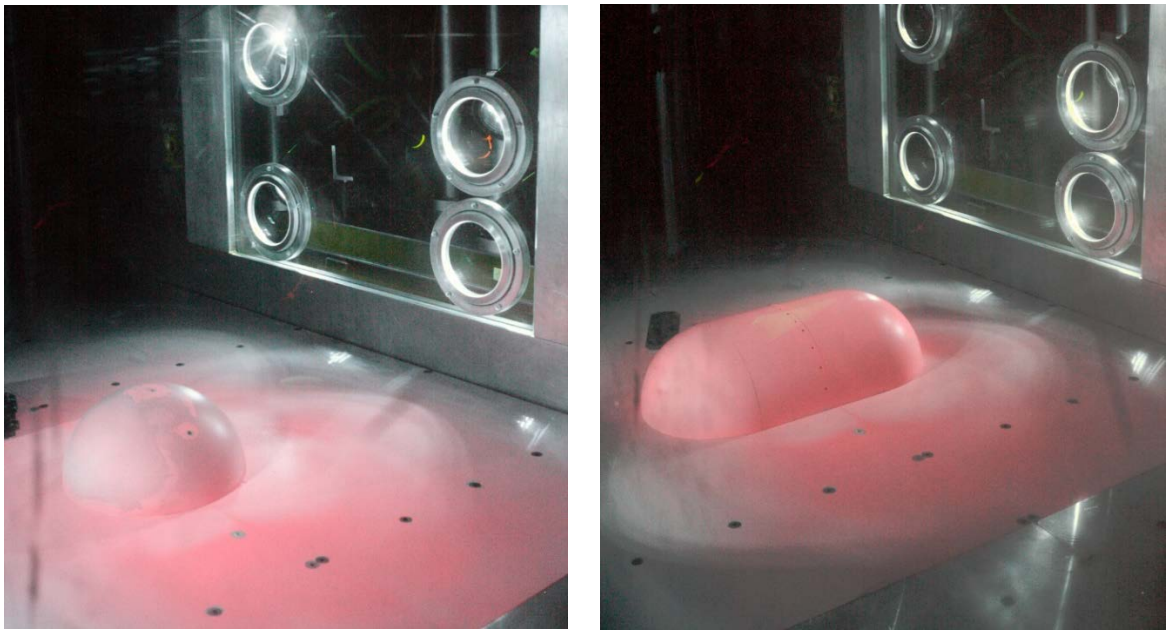

Figure 1. The tested turret geometries for PSP experiments. Left is the 8”-diameter hemisphere. Right is the 8”-diameter turret with AR = 1.87.

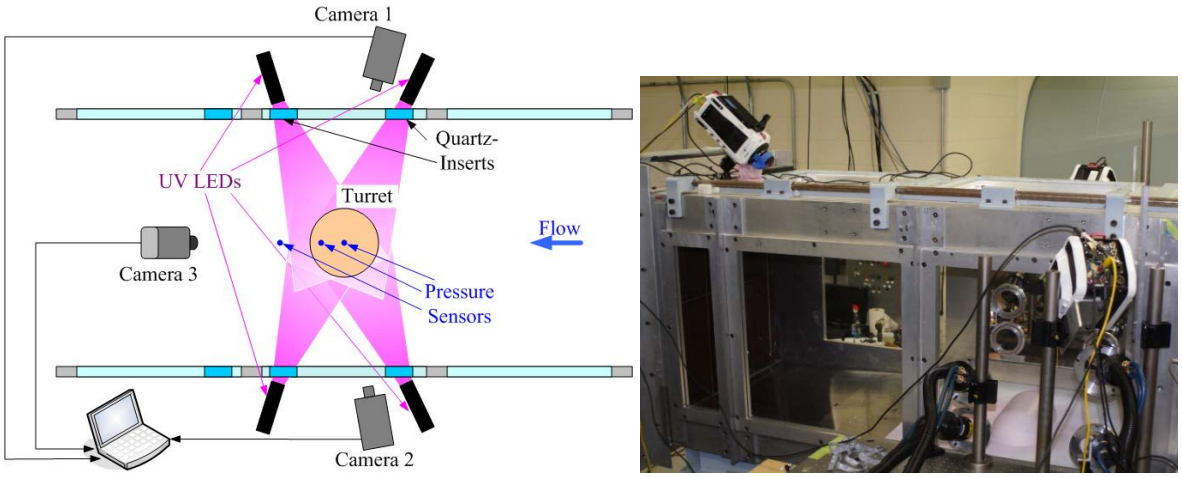

Figure 2. A schematic of the experimental setup, left and a picture, right.

Table 1: Geometric properties and run conditions of the turret configurations.

Configuration	Spanwise Length, *L*	Aspect Ratio (AR)	Incoming Mach Numbers*
Hemisphere	8”	1	0.41, 0.51, 0.57, 0.64, 0.66, 0.68
AR = 1.9	15”	1.9	0.42, 0.47, 0.53, 0.59, 0.63

Images were acquired at the framing rate of 3 kHz for 10,000 frames per each camera. The three cameras were triggered simultaneously, and the internal clocks were also synchronized. The unsteady pressure data were acquired at 30 kHz for 10 seconds. The unsteady pressure system was just triggered simultaneously because it was running at a higher sample rate.

III. Data Analysis

Before analysis was performed on the PSP images, the Kulite pressure sensors were used to calibrate the PSP response. This was done by first extracting a small patch of intensity data near a pressure port and spatially averaging over it to reduce noise, then comparing the instantaneous intensity variation to the pressure output from the pressure sensor. The known linear relationship between the intensity, $I(t)$, and pressure, $P(t)$ is given by

$$\frac{\overline{I(t)}}{I(t)} = 1 + AP(t)$$

where the overbar indicates a mean, and $P(t)$ is the *mean-removed* unsteady pressure. The A-constant was solved for by applying a linear fit to the normalized intensity ratio versus the mean removed pressure. The paint was found to correctly resolve the unsteady pressure spectrum up to the Nyquist frequency of 1,500 Hz, see Figure 3.

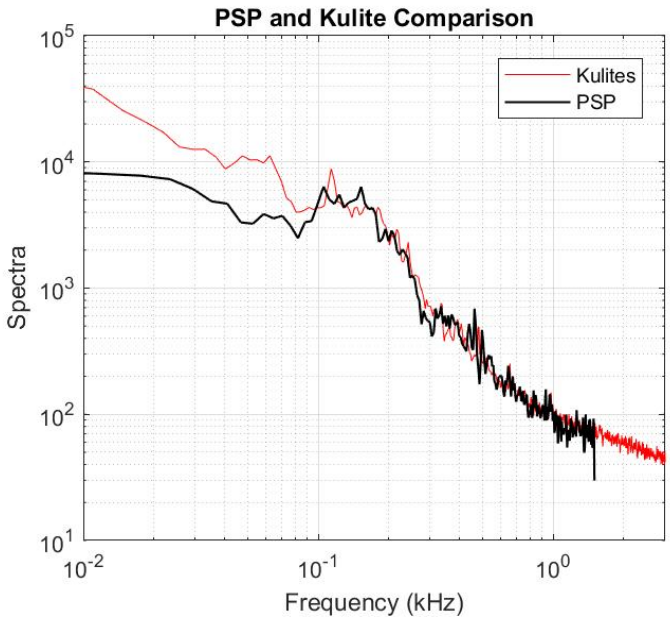

Figure 3. Power spectra of the unsteady pressure from the Kulite pressure sensor and PSP on top of the AR = 1.9 turret.

After converting the images into respective unsteady pressure fields, the data from all three cameras were used to reconstruct the full unsteady pressure field on the surface of the turret and around it on the tunnel wall, using Perspective Transformation Matrix (PTM) approach [3]. For the hemisphere, the signal from the Camera 3 (the top camera) was found to be very weak and noisy due to insufficient lighting, so images from only from Cameras 1 and 2 were used to reconstruct the unsteady pressure for the hemisphere.

Pressure values, both from global PSP data and local unsteady pressure sensors, were converted into Cp-fields using the corresponding freestream dynamic pressures, $q = 0.5\rho_\infty U_\infty^2$. All spatial coordinates were normalized by the radius of the streamwise curvature, R = 4 inches, which is the same for both geometries.

After spatio-temporal pressure fields were extracted, two modal decomposition techniques, Proper Orthogonal Decomposition (POD) and Dynamic Mode Decomposition (DMD), were used to analyze the dynamics and topology of the pressure fields.

POD represents the pressure field as a sum of orthogonal spatial modes, $\varphi_n(\vec{x})$, and the corresponding temporal coefficients, a_n,

$$P(\vec{x},t) = \sum_n a_n(t)\phi_n(\vec{x}) \tag{1}$$

The modes are arranged by the amount of energy in each mode, with the first mode having the largest percentage of the energy, the second mode having the second-largest energy and so on. To compute POD modes and the temporal coefficients, a widely-accepted algorithm using a Singular Value Decomposition (SVD) was used [25].

DMD decomposes the pressure field into spatial modes, Ψ_k, eigenvalues, λ_k, and the corresponding amplitudes, c_k,

$$P(\vec{x},t) = \sum_k c_k e^{\lambda_k t}\psi_k(\vec{x}) \tag{2}$$

The algorithm used to calculate DMD modes is described in detail in the companion paper [22]. Unlike POD modes, DMD modes are not orthogonal and complex, with the real and the imaginary parts, thus including any possible phase shifts between different spatial points. Thus, DMD analysis is beneficial when the flow has a convective component, with the corresponding phase differences. DMD modes are function of the frequency, as each DMD mode is computed for a fixed frequency, $\omega_k = \mathrm{Im}(\lambda_k)$. $|c_k|^2$ provides amount of spectral energy in each DMD mode.

IV. Results

For low subsonic speeds, the flow over the turret is fully subsonic. Due to blockage by the turret, the flow goes faster on top of the turret. When the incoming Mach number increases, the flow over the turret becomes locally supersonic, with a formation of an unsteady ending shock [12]. The Mach number when the flow reaches a sonic speed is called a critical Mach number. Using analytical Cp-distributions for inviscid incompressible flows, it was found that for the hemisphere, the critical Mach number is 0.55 [12], and for an infinite spanwise cylindrical turret the critical Mach number is 0.4. For the AR =1.9 turret, there is no analytical Cp-solution, but the critical Mach number should fall in between these critical Mach numbers and was estimated to be ~0.5.

While pressure fields were collected at multiple incoming Mach numbers, only two speeds were chosen in this paper to compare pressure fields for different turret geometries. The first speed corresponded to the speed slightly above the critical Mach numbers and it was M = 0.57 for the

hemisphere, and M = 0.53 for the AR = 1.9 turret. While technically for these speeds, the unsteady shock appears over the turret, the strength of the shock is very small, and it does not affect the pressure field; from the other hand, pressure fields are stronger at these incoming speeds, increasing signal-to-noise for PSP measurements. These incoming speeds will be referred as a subsonic case later in this paper.

The second chosen speed corresponded to the maximum reachable incoming speed, when the unsteady shock was the strongest for each geometry. For the hemisphere, it was M = 0.68, and for the AR = 1.9 turret, it was M = 0.63. These incoming speeds will be referred as a shock case later in this paper.

Spatial Cp_{rms}-fields

Spatial distributions of temporal root-mean-square, or $Cp_{rms}(x,y)$, were computed for both cases and geometries. The top view of Cp_{rms} fields for the hemisphere are presented in Figure 4, and the top view of Cp_{rms} fields for the AR = 1.9 turret are given in Figure 5. For the hemisphere for the subsonic case, Figure 4, left, the separation line, marked by the increased levels of the pressure fluctuations, is located at approximately x/R = 0.2, which corresponds to the separation angle of about 100 degrees. A similar location of the separation line at these subsonic speeds were observed using oil flow visualization in [13]. For the shock case, Figure 4, right, the shock prematurely trips the flow, resulting in the increased levels of Cp_{rms}; due to the tripping, the separation moves upstream to the location of about x/R = 0, or 90 degrees; the same results were observed in [13]. The relatively thin region of the increased pressure fluctuation indicates a small, within few degrees, spatial variation in the instantaneous shock location; similar conclusions were made based on the optical studies of the unsteady shock [6,26]. For both the subsonic and the shock cases, the separation line is approximately at the same spanwise location, except near the portions of the hemisphere close the tunnel wall, where the separation tends to move upstream, see the side view of the pressure fluctuations in Figure 5. These earlier separations near the tunnel wall were attributed to a formation of the vortical structures on both sides of the hemisphere [13]. Finally, the wake extent, denoted by the region of the increased pressure fluctuations downstream of the hemisphere, see Figure 4, is almost the same for the subsonic and the shock cases.

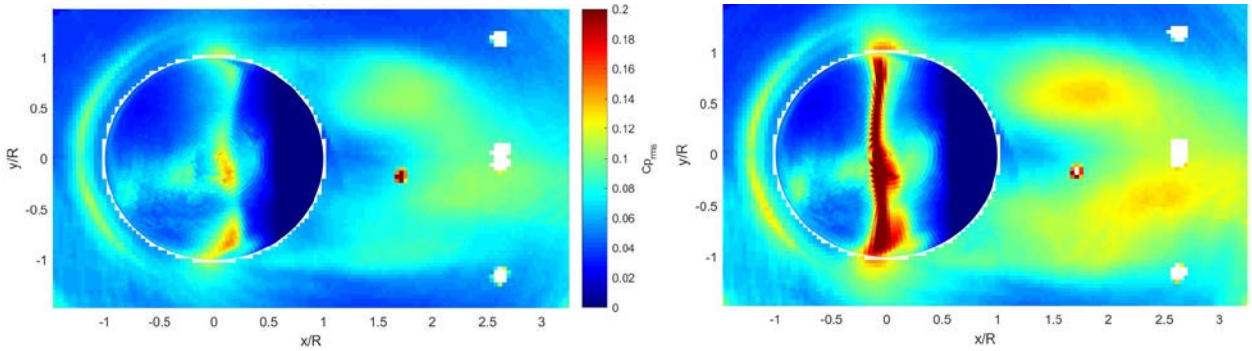

Figure 4. Top view of spatial distribution of Cp_{rms} for the hemisphere for (left) subsonic and (right) shock cases. Flow goes from left to right.

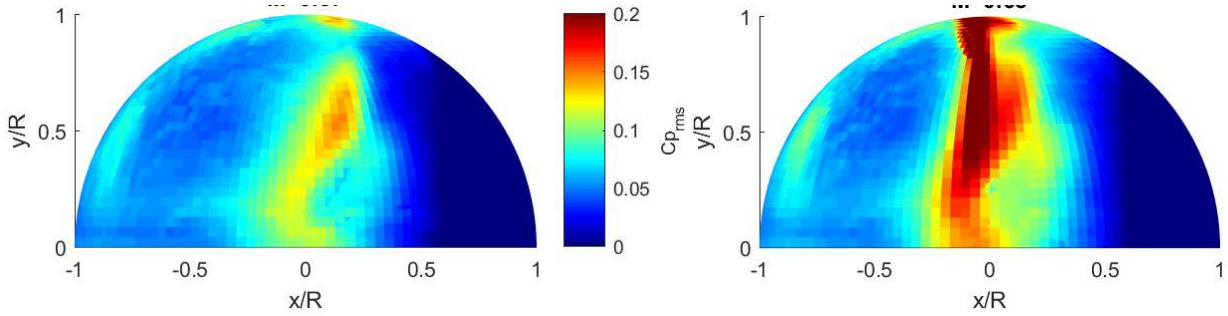

Figure 5. Side view of spatial distribution of Cp_{rms} for the hemisphere for (left) subsonic and (right) shock cases. Flow goes from left to right.

The spatial distributions of Cp_{rms} for the AR = 1.9 turret for both velocity cases are shown in Figure 6 (top view) and in Figure 7 (side view). For the subsonic case, Figure 6, left, and Figure 7, left, the flow still separates near x/R = 0.2 on the quarter-spherical portion of the turret, but separates earlier at x/R = 0 along the cylindrical portion of the turret. The formation of the unsteady shock over the turret also resulted in the increased pressure fluctuations on top of the turret, see Figure 6, right. The shock extent in the streamwise direction appears to be larger, compared to the hemisphere. Analysis of movies of the unsteady pressure field (not shown) has revealed that the shock forms at the downstream portion of the region of the increased pressure fluctuations and moves upstream, until it disappears in the beginning of the region. A similar, predominantly-upstream motion of the shock, but with a smaller streamwise extent, was also observed on the hemisphere and a possible physical mechanism was presented in [5]. The vortical structures near the tunnel wall, seen for the hemisphere in Figure 5, are much smaller and closer to the tunnel wall for the AR = 1.9 turret, see Figure 7.

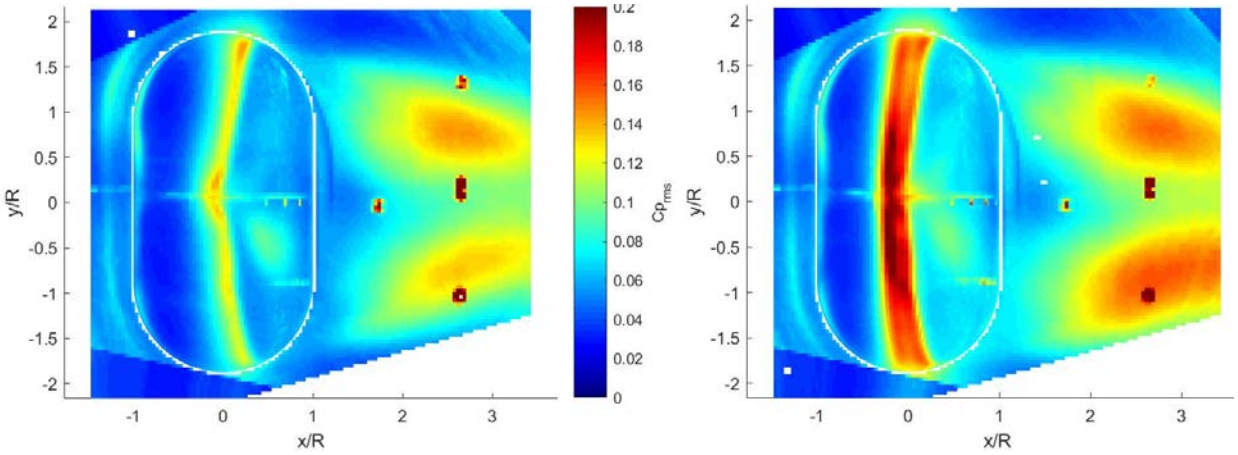

Figure 6. Top view of spatial distribution of Cp_{rms} for the AR = 1.9 turret for (left) subsonic and (right) shock cases. Flow goes from left to right.

The wake downstream of the AR = 1.9 turret is more energetic, as the Cp_{rms} values are close to 0.14, compared to Cp_{rms} ~ 0.1..0.12 for the hemisphere. As expected, the spanwise extent of the wake, defined as the y-distance between the maximum Cp_{rms} -values in the wake is larger, $\Delta y/R$ = 1.5, for the AR = 1.9 turret than for the hemisphere, $\Delta y/R$ = 1. However, the wake size, relative to the turret spanwise length, L, is smaller for the AR = 1.9 turret, $\Delta y/L$ = 0.55, than for the hemisphere, where $\Delta y/L$ = 0.75. Another way to see it is to compute the spanwise distance between

the end of the quarter-spherical cap of the turret along the spanwise direction and the y-location of the closest maximum Cp_{rms} in the wake. For the hemisphere, this distance is approximately 0.5R, while for the AR = 1.9 turret, it is closer to R.

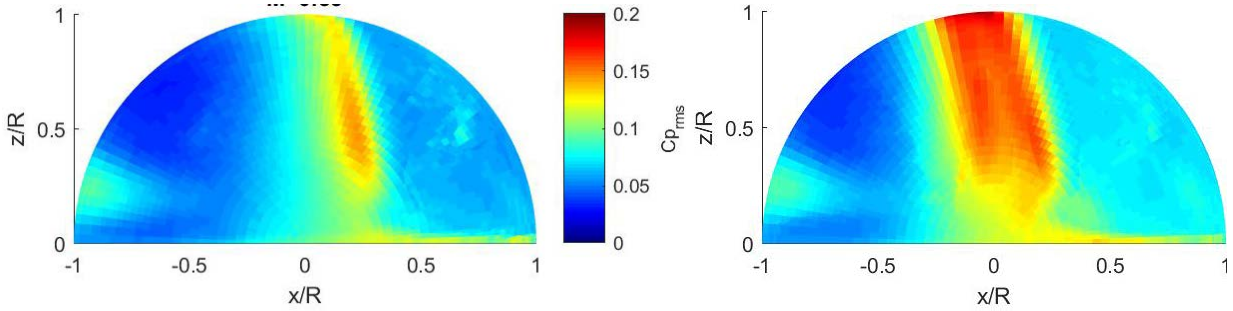

Figure 7. Top view of spatial distribution of Cp_{rms} for the AR = 1.9 turret for (left) subsonic and (right) shock cases. Flow goes from left to right.

To address the differences in the topology of the wake downstream of the hemisphere and the AR = 1.9 turret, it was discussed in the Introduction, that the spanwise curvature on both sides of the hemisphere is responsible for the formation of a pair of counter-rotating "horn" vortices downstream of the hemisphere [12]. These vortices affect the topology of the separated region, and, among other things, reduce the size of the separated region along the centerline, known as a "quiet valley" [6]. Since the same spanwise curvature is present on the quarter-spherical caps of the AR =1.9 turret, similar "horn" vortices are expected to form downstream of the quarter-spherical caps. Due to the larger spanwise extent of the AR = 1.9 turret, the "horn" vortices are farther separated in the spanwise direction, resulting in less interaction between them. As a consequence, the flow tends to separate later on these quarter-spherical caps near the tunnel wall, compare Figures 5 and 7. With the late separation, the separated flow near the tunnel wall has a momentum toward the turret centerline, resulting in the smaller relative wake extent for the AR = 1.9 turret.

POD analysis

While the presented analysis of Cp_{rms}-fields did reveal differences in the spatial distribution of time-averaged pressure fluctuations, it did not provide any information about the changes in the dynamics of the pressure fields for both geometries. To study these dynamical changes, POD modes were computed only on the surfaces of the turrets, excluding the pressure data at the tunnel wall around the turrets.

The first three POD modes for the hemisphere for the subsonic case are shown in Figure 8. Detailed analysis of the POD modes and their physical meanings is given in [21,22], so only relevant results will be briefly discussed here. The first POD mode holds 45% of the total pressure "energy" and mostly anti-symmetric in the spanwise direction. This mode was found to correspond to the wake shifting mode, when the whole wake repeatedly shifts in the spanwise direction [21]. The second mode is mostly spanwise-symmetric and corresponds to the wake breathing in the vertical direction [21]. Finally, the third POD mode is also spanwise-symmetric and corresponds to the wake breathing in the spanwise direction [21]. Together, these three modes are responsible for 65% of the total pressure "energy" on the surface of the hemisphere.

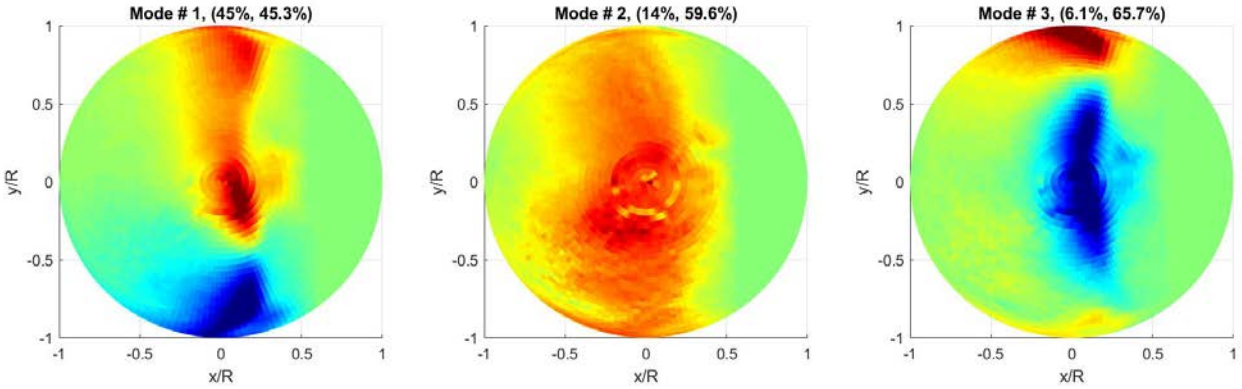

Figure 8. The first 3 dominant POD modes for the hemisphere for the subsonic case. The corresponding normalized and the cumulative energies for each POD mode are given as a first and a second number in parenthesis. Flow goes from left to right.

The first three POD modes for the AR = 1.9 turret for the subsonic case are shown in Figure 9. The first mode is anti-symmetric in the spanwise direction and qualitatively is very similar to the first hemispheric POD mode; however, it holds only 28% of the pressure "energy". The second mode is symmetric in the spanwise direction and is similar to the third hemispheric POD mode. The third POD mode is also spanwise-symmetric and resembles the second hemispheric POD mode. Between of the first three POD modes, they contain about 46% of the pressure "energy". The analysis of the cumulative energy of the POD modes (not shown) revealed that for the hemisphere, 80% of the total pressure "energy" is in the first 30 modes, while it takes almost 50 modes for the AR = 1.9 turret to reach the same value of 80%. All of it indicates that the pressure field on the AR = 1.9 turret is less organized than the pressure field over the hemisphere and it can be contributed to the decreased interaction between the "horn" vortices. Thus, closer separation between the "horn" vortices for the hemisphere is responsible for a more organized pressure field on the hemisphere.

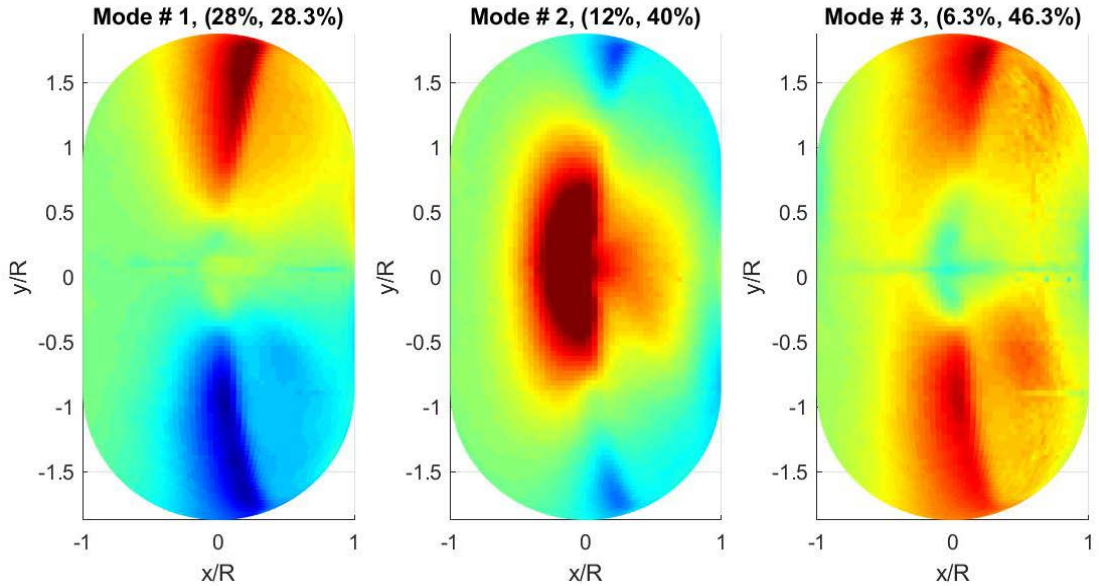

Figure 9. The first 3 dominant POD modes for the AR = 1.9 turret for the subsonic case. The corresponding normalized and the cumulative energies for each POD mode are given as a first and a second number in parenthesis. Flow goes from left to right.

Power spectra of the temporal coefficients for the first three POD modes for both geometries are presented in Figure 10. Most of the energy for the hemispheric modes is located at low, $St_D < 0.3$, frequencies, see Figure 10, left. The spectral energy of the first POD mode for the AR = 1.9 turret, Figure 10, right, is centered near lower frequencies below $St_D = 0.2$, with a wide peak at $St_D = 0.1$. This peak indicates more regularized flow dynamics, compared to the dynamics of the first hemispheric mode. Also, the first POD mode for the AR = 1.9 turret, which is related to the wake shifting in the spanwise direction, has a lower frequency content, than the first hemispheric POD mode.

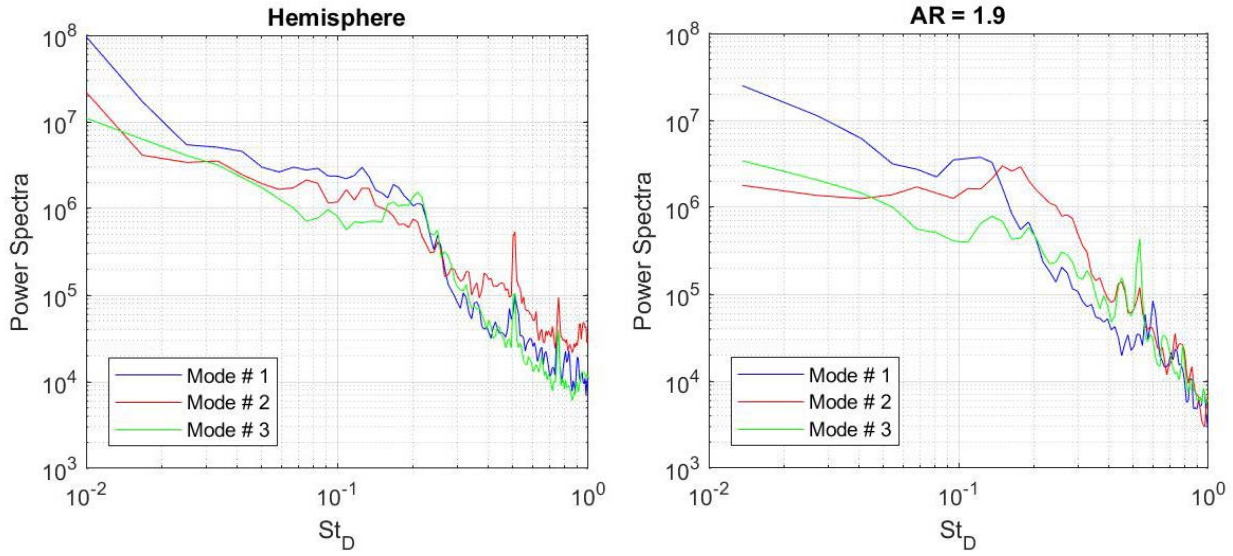

Figure 10. Spectra for temporal coefficients for first three POD modes for the hemisphere (left) and for the AR = 1.9 turret (right) for the subsonic case. Frequency is normalized by the streamwise diameter, D = 2R, and the incoming speed, $St_D = fD/U_\infty$.

As the wake spatial spanwise extent gets larger for the AR = 1.9 turret, it is plausible that a proper parameter in the dynamics of the wake shifting is the spanwise dimension of the turret, L. To check it, the spectra for the first POD modes for both the hemisphere and the AR = 1.9 turret are plotted as a function of $St_L = fL/U_\infty$ and presented in Figure 11. The spectral peaks are still not aligned, as the spectral peak for the AR = 1.9 turret is now at $St_L = 0.2$, so the dynamics of the wake shifting mode might depend on both the streamwise and the spanwise extents of the turret for the subsonic speed. As it will be shown later, the spectra exhibit a better collapse with St_L for the shock case.

As discussed above, the second POD mode for the AR = 1.9 turret is spatially similar to the third hemispheric POD mode, and the corresponding spectra both have a peak near StD = 0.2. The spectra for the third POD mode and the similar second hemispheric POD mode also look similar, with the peak in the spectra around $St_D = 0.2$. As these modes are related to the wake breathing mode, the dynamics of this breathing mode is related to the streamwise length, D, of the turret.

For the shock case, the first POD modes for the hemisphere are shown in Figure 12. The presence of the unsteady shock is clearly visible in POD modes. Similar to the subsonic case, the first POD mode is also mostly anti-symmetrical in the spanwise direction, and the second and the third modes are predominantly spanwise-symmetric; all three modes are responsible for the 63% percent of the unsteady pressure “energy”.

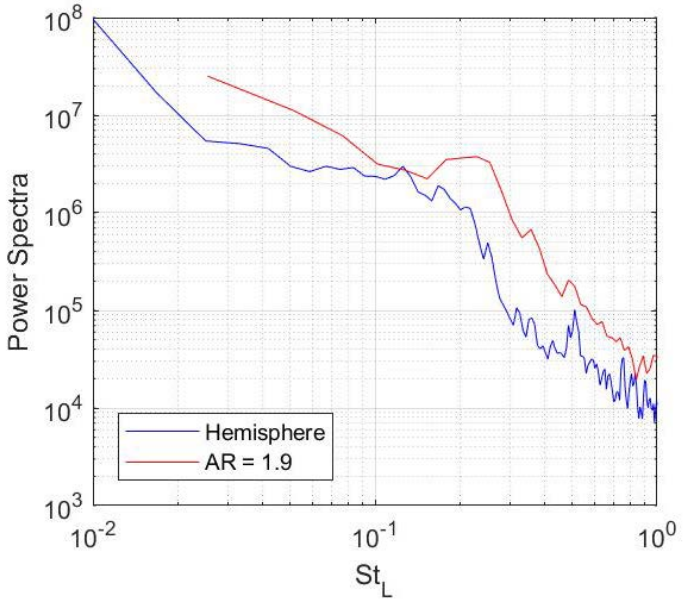

Figure 11. Spectra for temporal coefficients for the first POD mode for the hemisphere and for the AR = 1.9 turret for the subsonic case. Frequency is normalized by the spanwise length, L, $St_L = fL/U_\infty$.

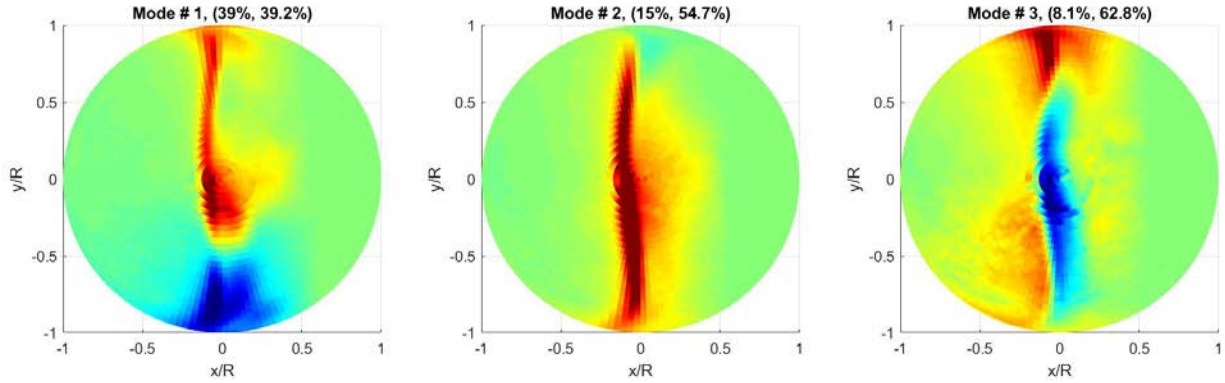

Figure 12. The first 3 dominant POD modes for the hemisphere for the shock case. The corresponding normalized and the cumulative energies for each POD mode are given as a first and a second number in parenthesis. Flow goes from left to right.

The first three POD modes for the AR = 1.9 turret are given in Figure 13. The first POD is also anti-symmetric, and the two other modes are symmetric in the spanwise direction. The shock on top of the turret has a regularizing effect on the flow over the turret, as the large non-zero values in the first two POD modes, indicating non-zero cross-correlations, extend along a larger portion of the turret in the spanwise direction, compared to the subsonic case in Figure 9. The shock-regularizing effect is also responsible for the increased, up to 52%, amount of pressure "energy" in the first POD modes, compared to 46% for the subsonic case.

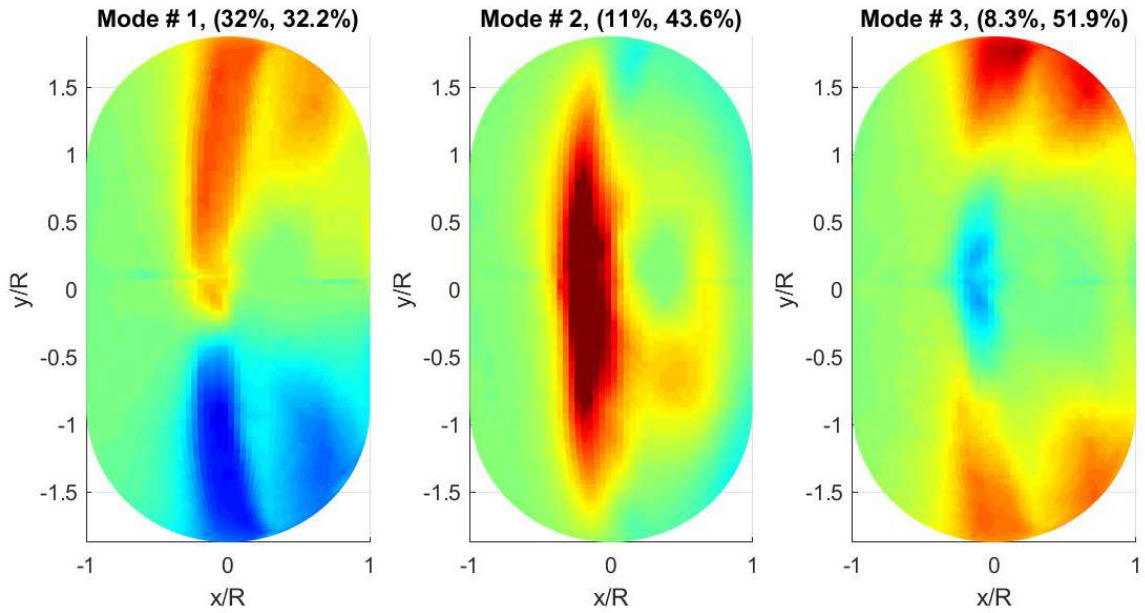

Figure 13. The first 3 dominant POD modes for the AR = 1.9 turret for the shock case. The corresponding normalized and the cumulative energies for each POD mode are given as a first and a second number in parenthesis. Flow goes from left to right.

The power spectra of the temporal coefficients of the dominant POD modes for both geometries are plotted in Figure 14. The presence of the shock regularizes the modes' dynamics, as indicated by the appearance of wide spectral peaks at $St_D = 0.2$ for the hemisphere, Figure 14, left. The spectra for the first POD modes for the AR = 1.9 turret are shown in Figure 14, right. The location of the dominant spectral peak for the first POD mode is shifted toward a lower frequency of $St_D = 0.1$. When the spectra of the first POD modes for both geometries are plotted versus St_L, shown in Figure 15, the spectral peaks are now aligned at $St_L = 0.2$. So, for the shock case, the dynamics of the first POD mode seems to be dependent on the spanwise length of the turret, and not the streamwise length.

Spectral peaks for the second and the third modes for both geometries are still near $St_D = 0.2$, see Figure 14. It confirms that for both subsonic and the shock cases, the wake breathing mode, related to the second and the third POD modes, depends primarily on the streamwise extent of the turret.

Overall, POD analysis of the unsteady pressure fields for both geometries and the incoming speed cases had revealed that the dominant pressure mode on the surface of the turret is anti-symmetric in the spanwise direction, indicating that the dominant wake motion is the wake shifting. The dominant frequency of the wake shifting is related to the spanwise extent of the turret, with high frequencies for the hemisphere and lower frequencies for the AR = 1.9 turret. Another dominant wake mode is the wake breathing mode and it is present for both turret geometries. The dominant frequency of this mode appears to depend on the streamwise length of the turret.

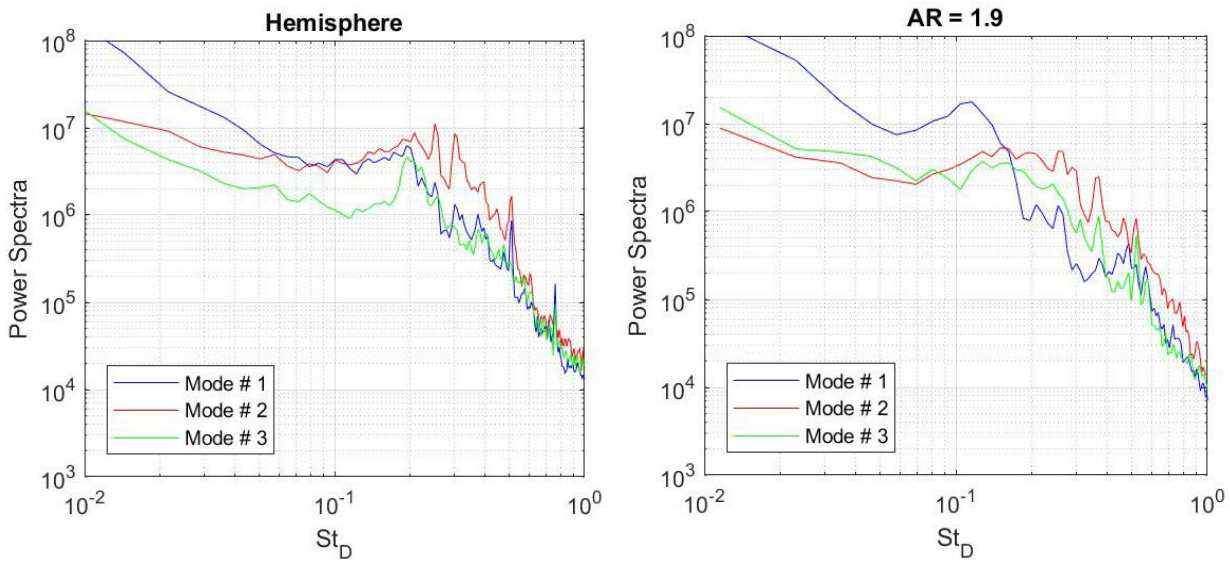

Figure 14. Spectra for temporal coefficients for first three POD modes for the hemisphere (left) and for the AR = 1.9 turret (right) for the shock case. Frequency is normalized by the streamwise diameter, D =2R, and the incoming speed. Frequency is normalized by the streamwise diameter, D =2R, and the incoming speed, $St_D = fD/U_\infty$.

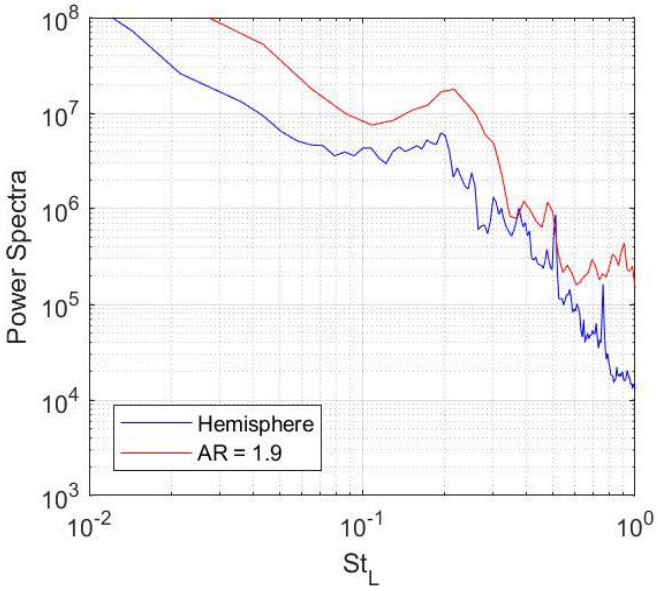

Figure 15. Spectra for temporal coefficients for the first POD mode for the hemisphere and for the AR = 1.9 turret (right) for the shock case. Frequency is normalized by the spanwise length, L, $St_L = fL/U_\infty$.

The presence of the shock has a regularizing effect of the flow dynamics around the turrets, as the cross-correlations on tops of the turrets are increased near the shock location and the spectra of the dominant POD modes starts exhibiting well-defined peaks in the range of normalized frequencies of St_D = 0.1..0.2. Similar conclusions were made analyzing the correlations between the shock motion and the unsteady pressures in the wake downstream of the hemisphere at different subsonic and transonic speeds in-flight [23].

DMD analysis

Analysis of the POD modes for the full pressure fields on and around the turrets was also performed, but did not reveal any clear trends in wake dynamics between both turret geometries and therefore is not presented here. One reason this the lack of clear trends is that POD decomposition relies on *instantaneous* cross-correlations among different spatial points and therefore does not take into account a convective nature of the structures in the wake. DMD modes, as discussed before, have both the real and the imaginary parts, and can provide valuable information about the topology and dynamics of convective structures.

Detailed analysis of DMD modes for the hemisphere is presented in [22]. Based on this analysis, normalized frequencies of St_D = 0.15 and 0.2 were chosen as representative frequencies of the unsteady pressure field for the subsonic and shock cases, respectively, and the corresponding complex DMD modes were calculated for the subsonic and the shock cases.

The real and the imaginary part of the DMD mode at St_D = 0.15 for the hemisphere for the subsonic case is shown in Figure 16. As all three dominant POD modes are present at this frequency, the DMD mode is essentially a combination of first dominant POD modes. Both parts of the DMD mode appear to be mostly spanwise anti-symmetric, as the first POD mode is still a dominant one at this frequency, see Figure 10.

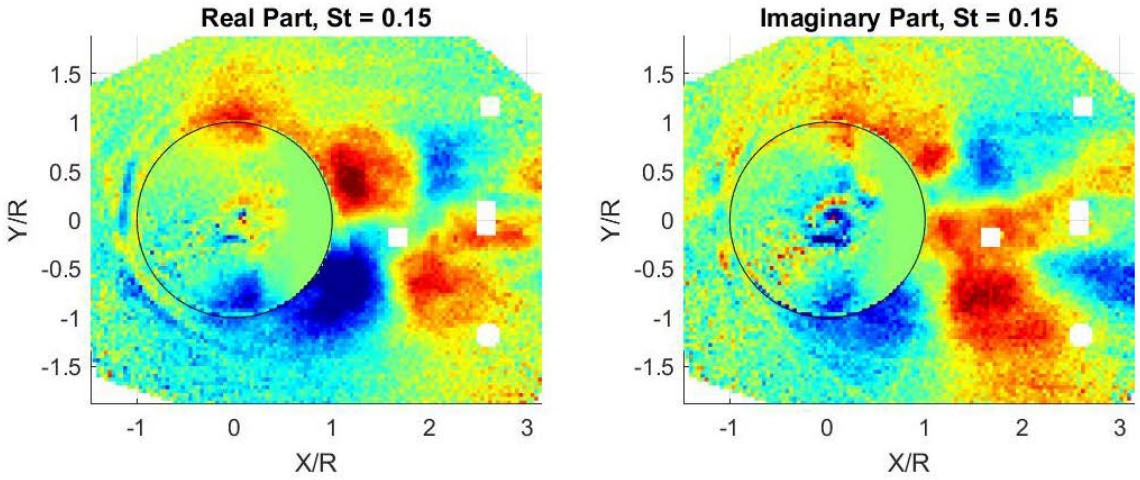

Figure 16. Real (left) and imaginary (right) parts of the DMD mode at StD = 0.15 for the hemisphere for the subsonic case. Flow goes from left to right.

As mentioned before, DMD mode preserves the phase information between various spatial points, so it can identify regions with predominantly convecting structures. For instance, if the portion of the wake between x/R = 0 .. 3 and y/R = -1.5 .. -0.5 is compared for both the real and the imaginary parts in Figure 16, the pressure field appears to be simply shifted in the streamwise direction by approximately $\Delta x/R = 0.5$; the same can be seen for the other side of the wake, /R = 0.5 .. 1.5. It indicates that the pressure field convects on both sides on the wake and the convecting structures are correlated to the dynamic of the separation region of both sides of the hemisphere. Using this information, in [22] the convective speed of the structures was estimated to be approximately $0.5U_\infty$ for the subsonic case.

DMD mode for the dominant frequency of StD = 0.2 for the shock case is presented in Figure 17. The wake features are approximately the same for the shock case, compared to the subsonic case, with the mode being a predominantly spanwise anti-symmetric. As the shock causes the premature separation closer to the apex of the hemisphere, the wake is slightly wider in the

spanwise direction. The increased values of DMD mode near the shock on top of the turret indicates the increased correlation between the unsteady shock and the wake dynamics, consistent with similar findings in [23].

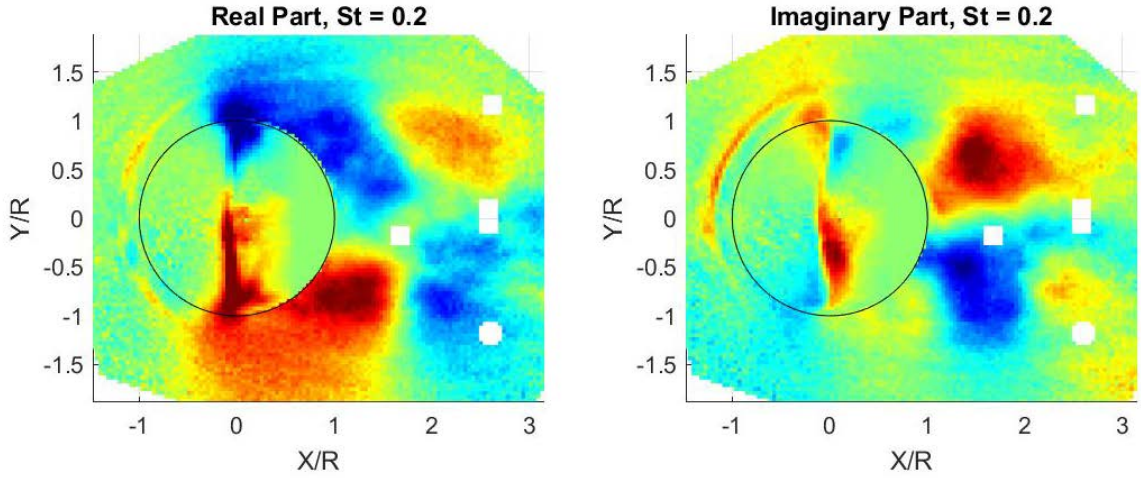

Figure 17. Real (left) and imaginary (right) parts of the DMD mode at StD = 0.2 for the hemisphere for the shock case. Flow goes from left to right.

Similar DMD analysis for performed for the full pressure field on and around the AR = 1.9 turret. DMD energies for different frequencies, $|c_k|^2$, for both the subsonic and the shock cases are presented in Figure 18. Based on these results, the dominant frequency of the unsteady pressure field for the subsonic case was found to be St_D = 0.13. For the shock case, two dominant frequencies were identified, St_D = 0.15 and 0.27.

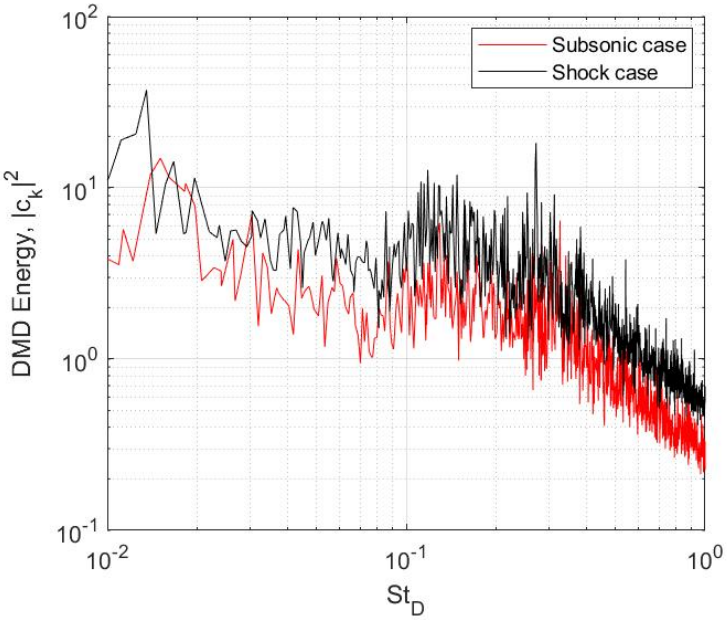

Figure 18. DMD energies as a function of St_D for the AR =1.9 turret for the subsonic and the shock cases.

The DMD mode for St_D = 0.13 for the subsonic case is presented in Figure 19. The mode is qualitatively similar the DMD mode for the hemisphere for the subsonic case, seen in Figure 16, showing mostly spanwise anti-symmetric feature and the presence of the convecting structures in the wake. As for the differences between these two DMD modes, the structure size in the streamwise direction is larger for the AR = 1.9 turret. Also, the wake gets narrower farther downstream of the turret, consistent with similar conclusions, made earlier in this paper. Increased amplitudes of the DMD mode near the top of the turret confirms the increased correlation between the separation on the turret and the wake dynamics.

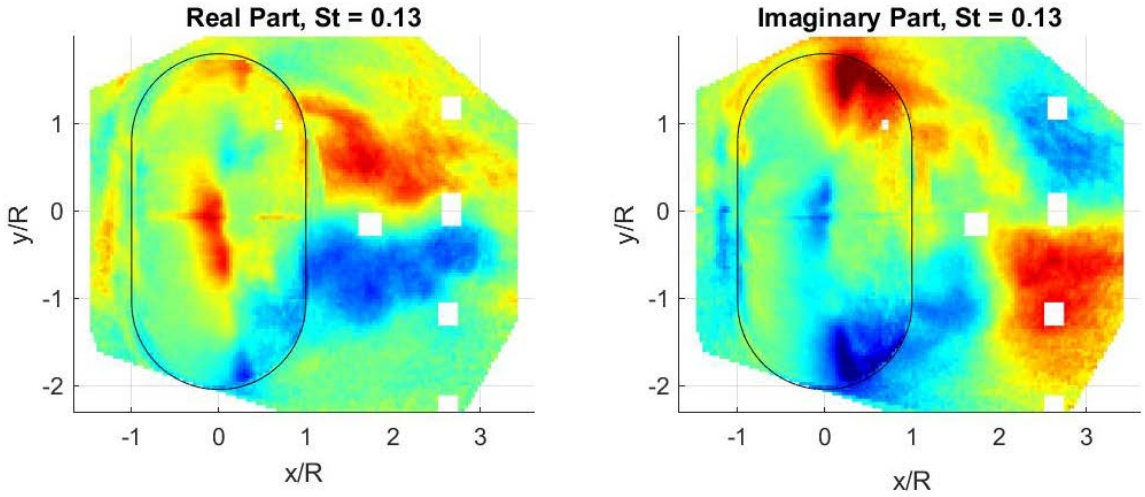

Figure 19. Real (left) and imaginary (right) parts of the DMD mode at StD = 0.13 for the AR = 1.9 turret for the subsonic case. Flow goes from left to right.

The DMD mode for St_D = 0.15 for the shock case is presented in Figure 20. The wake topology is very similar to the one for the subsonic case. The shock motion is strongly correlated with the wake motion, as indicated by the increased amplitudes of the DMD mode near the top of the turret.

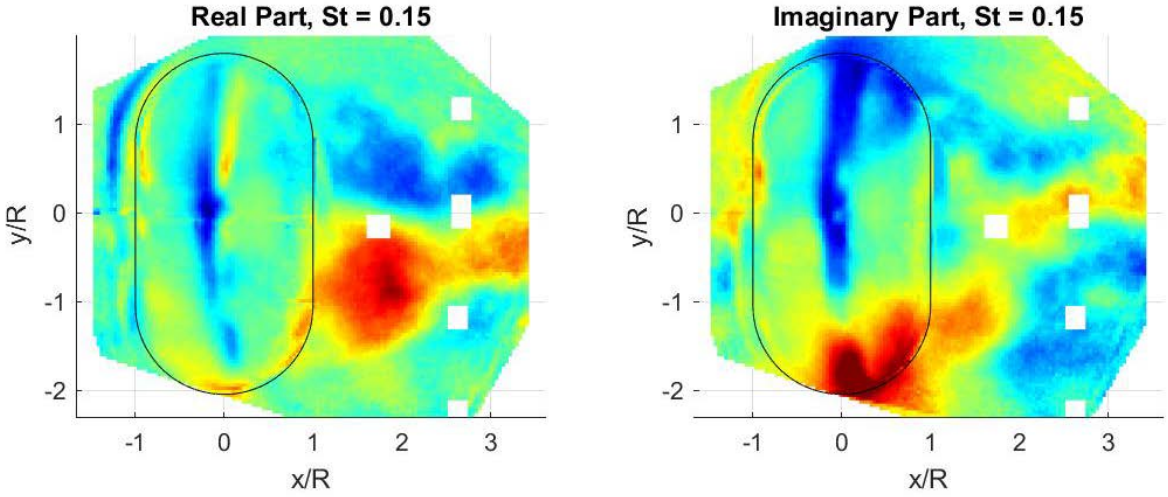

Figure 20. Real (left) and imaginary (right) parts of the DMD mode at StD = 0.13 for the AR = 1.9 turret for the shock case. Flow goes from left to right.

The DMD mode for another dominant frequency of St_D = 0.27 are presented in Figure 21. At this frequency, the dominant POD mode is the second POD mode, see Figure 14, so the DMD

mode is expected to mostly spanwise-symmetric. Indeed, that is the case, seen in Figure 21, where DMD mode on the turret and in the wake is spanwise-symmetric. The wake also revealed the presence of the convecting structures, which are strongly correlated to the shock motion. As this DMD mode is related to the second DMD mode, this DMD mode corresponded to the vertical wake breathing mode.

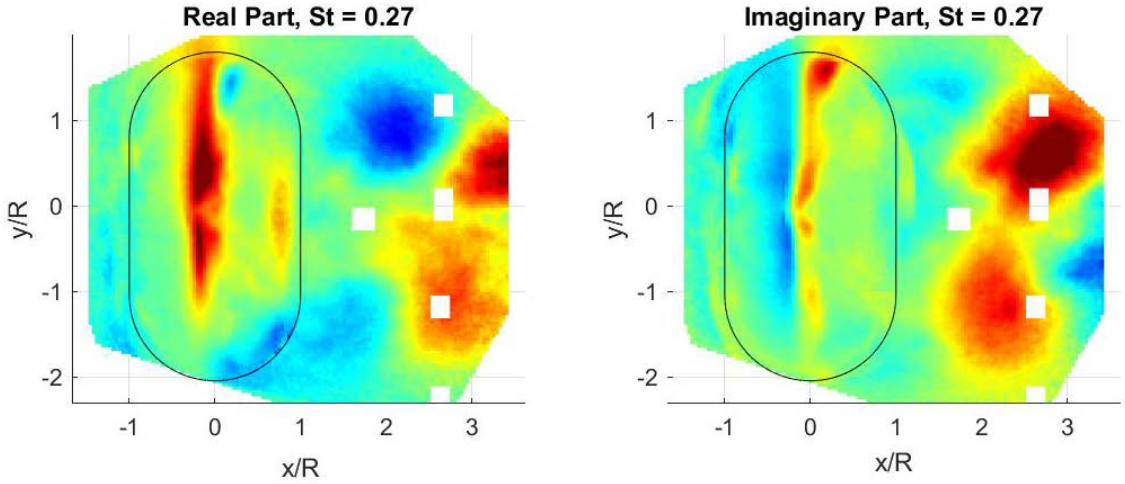

Figure 21. Real (left) and imaginary (right) parts of the DMD mode at StD = 0.27 for the AR = 1.9 turret for the shock case. Flow goes from left to right.

In summary, DMD analysis revealed changes in the topology of the wake for the AR = 1.9 turret, such as the narrowing wake and larger traveling structures, compared to the wake downstream of the hemisphere. Results are consistent with Cp_{rms}-field analysis, presented earlier, and also concludes that the interaction between the "horn" vortices, formed downstream of the quarter-spherical caps, affects the wake dynamics and the topology. This analysis provides additional information about the dynamics of the wake and will be used in the future work to develop a low-dimensional model of the wake dynamics and the shock-wake interaction.

V. Conclusions

A fast-response pressure-sensitive paint was used to measure unsteady pressure fields on and around two different turret geometries: the hemisphere and the turret, consisted of two quarter-spherical caps with a cylindrical insert in between. Both geometries have the same streamwise curvature of the radius of 4", but the second geometry has a larger spanwise extent of 15", or the aspect ratio of 1.9. Measurements were conducted in a close-loop tunnel at various subsonic and transonic speeds. The paint was illuminated with multiple UV-light sources and the instantaneous fluorescence intensity was measured by three high-speed cameras with a sampling rate of 3 kHz.

By separating the quarter-spherical caps in the spanwise direction, the spanwise distance between the "horn" vortices, formed downstream of these quarter-spherical caps, was larger for the second turret geometry. As a consequence, the far-field interaction between two "horn" vortices was reduced. So, while the streamwise curvature, which is responsible for the flow separation off the turret, was the same for both turret geometries, a combined effect of both "horn" vortices" on the wake dynamics were different between the two geometries.

Two modal techniques, Proper Orthogonal Decomposition and Dynamic Mode Decomposition, were used to analyze the topology and the dynamics of the wake for both turrets at different speeds. At fully subsonic speeds, the first three POD modes were found to contain 65% of the total pressure

"energy". At higher transonic speeds, an unsteady shock is formed over the hemisphere, which was shown to have an organizing effect on the pressure field, evidenced by the appearance of spectral peaks in the spectral content of the dominant POD modes. Analysis of the pressure variations in the wake downstream of the hemisphere revealed the presence of the traveling structures. These structures were correlated with the unsteady separation on the hemisphere.

When the "horn" vortices were separated farther for the second turret geometry, the decreased interaction between them have several effects on the wake dynamics. The separation off the quarter-spherical caps was delayed, resulted in the narrowing wake farther downstream of the turret and the increased size of the convecting structures. The combined energy in the first three POD modes were 46%, which is less than for the hemisphere. The dominant peak frequency of the first POD mode, which is related to the wake shifting motion, was observed at a smaller normalized frequency, when normalized with the curvature radius. When the spanwise extent of the turret was used to normalize frequencies, spectra for the first POD modes for both turret geometries were found have a better collapse. This indicates that the wake shifting motion depends on the spanwise extent of the turret, and not the streamwise curvature. The presence of the shock at higher transonic speeds was also found to have a regularizing effect on the wake for both turret geometries.

The second and the third POD modes for both geometries are related to the wake breathing mode. Analysis of the spectra of these POD modes revealed that the dynamics of the wake breathing mode is related to the radius of the streamwise curvature.

Acknowledgments

This work is supported by the Joint Technology Office, Grant number FA9550-13-1-0001. The U.S. Government is authorized to reproduce and distribute reprints for governmental purposes notwithstanding any copyright notation thereon.

The authors also would like to thank Thomas Juliano for his help painting the models with PSP and Steve Palluconi from Innovative Scientific Solutions, Inc (ISSI) for many useful discussions and recommendations about using PSP.

References

[1] Snyder, C.H., Franke, M.E., Masquelier, M.L., "Wind-Tunnel Tests of an Aircraft Turret Model", Journal of Aircraft,37(3), pp. 368-376, 2000.

[2] Sluder, R., Gris, L., Katz, J., "Aerodynamics of a Generic Optical Turret", Journal of Aircraft, 45(5), pp. 1814-1815,2008.

[3] Gordeyev, S., De Lucca, N., Jumper, E.J., Hird, K., Juliano, T.J., Gregory, J.W., Thordahl, J., and Wittich, D.J., "Comparison of Unsteady Pressure Fields on Turrets with Different Surface Features using Pressure Sensitive Paint", Experiments in Fluids, 55, p. 1661, 2014.

[4] Porter C., Gordeyev, S., Zenk, M., and Jumper, E.J., "Flight Measurements of the Aero-Optical Environment around a Flat-Windowed Turret", AIAA Journal, 51(6), pp. 1394-1403, 2013.

[5] De Lucca, N., Gordeyev, S., and Jumper, E.J., "In-flight aero-optics of turrets", Journal of Optical Engineering, 52(7), 071405, 2013

[6] J. Morrida, S. Gordeyev and E. Jumper, "Transonic Flow Dynamics Over a Hemisphere in Flight", AIAA Paper 2016-1349, 2016.

[7] E. Mathews, K. Wang, M. Wang and E. Jumper, "LES of an Aero-Optical Turret Flow at High Reynolds Number", AIAA 2016-1461, 2016.

[8] R. Jelic, S. Sherer and R.Greendyke, “Simulation of Various Turret Configurations at Subsonic and Transonic Flight Conditions Using OVERFLOW”, Journal of Aircraft, 50, pp. 398-409, 2013.
[9] Coirier, W.J, Porter, C., Barber, J., Stutts, J., Whiteley, M., Goorskey, D. and Drye, R.,”Aero-Optical Evaluation of Notional Turrets in Subsonic, Transonic and Supersonic Regimes,” AIAA Paper 2014-2355, 2014
[10] P.E. Morgan and M.R. Visbal, “Hybrid Reynolds-Averaged Navier–Stokes/Large-Eddy Simulation Investigating Control of Flow over a Turret,” Journal of Aircraft, Vol. 49, No. 6, pp. 1700-1717, 2012.
[11] Ladd, J., Mani, A. and Bower, W., “Validation of Aerodynamic and Optical Computations for the Unsteady Flow Field About a Hemisphere-on-Cylinder Turret,” AIAA Paper 2009-4118, 2009.
[12] S. Gordeyev and E. Jumper, "Fluid Dynamics and Aero-Optics of Turrets", Progress in Aerospace Sciences, 46, (2010), pp. 388-400.
[13] S. Gordeyev, A. Vorobiev, E. Jumper, S. Gogineni and D.J. Wittich, “Studies of Flow Topology around Hemisphere at Transonic Speeds Using Time-Resolved Oil Flow Visualization”, AIAA Paper 2016-1459, 2016.
[14] A. Vorobiev, S. Gordeyev, E. Jumper, S. Gogineni, A. Marruffo and D.J. Wittich, “Low-Dimensional Dynamics and Modeling of Shock-Separation Interaction over Turrets at Transonic Speeds,” AIAA Paper 2014-2357, 2014.
[15] S. Gordeyev, J.A. Cress, E. Jumper and A.B. Cain, "Aero-Optical Environment Around a Cylindrical Turret with a Flat Window", *AIAA Journal*, Vol. 49, No. 2, pp. 308-315, 2011.
[16] K. Wang, M. Wang, S. Gordeyev and E. Jumper "Computation of Aero-Optical Distortions over a Cylindrical Turret with Passive Flow Control", 41th AIAA Plasmadynamics and Lasers Conference, AIAA Paper 2010-4498, 2010.
[17] Liu T, Campbell BT, Burns SP, Sullivan JP, “Temperature- and pressure-sensitive luminescent paints in aerodynamics,” Appl. Mech. Rev. 50(4), pp.227–246, 1997.
[18] Gregory JW, Asai K, Kameda M, Liu T, Sullivan JP, “A review of pressure-sensitive paint for high-speed and unsteady aerodynamics, “ Proc Inst Mech Eng G J Aerosp 222(2), pp. 249–290, 2008.
[19] S. Fang, S,R. Long, K,J. Disotell, J,W. Gregory, F,C. Semmelmayer, and R.W. Guyton, “Comparison of Unsteady Pressure-Sensitive Paint Measurement Techniques,” AIAA Journal, 50(1), pp. 109-122, 2012.
[20] S. Fang, K. J. Disotell, S.R. Long, J.W. Gregory, F.C. Semmelmayer, and R.W. Guyton, “Application of fast-responding pressure-sensitive paint to a hemispherical dome in unsteady transonic flow,” Experiments in Fluids 50, pp. 1495–1505, 2011.
[21] S. Gordeyev, N. De Lucca, J. Morrida, E.J. Jumper, and D.J. Wittich, “Conditional Studies of the Wake Dynamics Downstream of Hemispherical Turret Using PSP,” AIAA Paper 2018-2048, 2018.
[22] N. De Lucca, S. Gordeyev, J. Morrida, E.J. Jumper, and D.J. Wittich, “Modal Analysis of the Surface Pressure Field Around a Hemispherical Turret using Pressure Sensitive Paint,” AIAA Paper 2018-0932, 2018.
[23] J. Morrida, N. De Lucca, S. Gordeyev, and E.J. Jumper, “Simultaneous Pressure and Optical Measurements Around Hemispherical Turret in Subsonic and Transonic Flight”, AIAA Paper 2017-3654, 2017.

[24] S.J. Beresh, J.F. Henfling, R.W. Spillers, and B.O.M. Pruett, “Unsteady Shock Motion in a Transonic Flow over a Wall-Mounted Hemisphere”, AIAA Paper 2013-3201, 2013.
[25] K. Taira, S.L. Brunton, S.T.M. Dawson, C.W. Rowley, T. Colonius, B.J. McKeon, O.T. Schmidt, S. Gordeyev, V. Theofilis, and L.S. Ukeiley, "Modal Analysis of Fluid Flows: An Overview", AIAA Journal, 2017, https://doi.org/10.2514/1.J056060
[26] J. Morrida, S. Gordeyev, E.J. Jumper, S. Gogineni and D.J. Wittich, “Investigation of Shock Dynamics on a Hemisphere Using Pressure and Optical Measurements, ” AIAA Paper 2016-1348, 2016.